



HAL
open science

One spiro to shift them all: tuning fluorescent organic nanoparticles emission via steric design

Eléonore Kurek, Ophélie Dal Pra, Aliocha Skrzypczak, Stéphane Massip, Jonathan Daniel, Mireille Blanchard-desce, Chloé Grazon

► **To cite this version:**

Eléonore Kurek, Ophélie Dal Pra, Aliocha Skrzypczak, Stéphane Massip, Jonathan Daniel, et al.. One spiro to shift them all: tuning fluorescent organic nanoparticles emission via steric design. *Chemical Communications*, In press, <10.1039/d5cc06995e>. <hal-05518928>

HAL Id: hal-05518928

<https://hal.science/hal-05518928v1>

Submitted on 19 Feb 2026

HAL is a multi-disciplinary open access archive for the deposit and dissemination of scientific research documents, whether they are published or not. The documents may come from teaching and research institutions in France or abroad, or from public or private research centers.

L'archive ouverte pluridisciplinaire **HAL**, est destinée au dépôt et à la diffusion de documents scientifiques de niveau recherche, publiés ou non, émanant des établissements d'enseignement et de recherche français ou étrangers, des laboratoires publics ou privés.



Distributed under a Creative Commons CC BY 4.0 - Attribution - International License

ChemComm

Chemical Communications

Accepted Manuscript

This article can be cited before page numbers have been issued, to do this please use: E. KUREK, O. Dal Pra, A. Skrzypczak, S. Massip, J. Daniel, M. Blanchard-Desce and C. Grazon, *Chem. Commun.*, 2026, DOI: 10.1039/D5CC06995E.



This is an Accepted Manuscript, which has been through the Royal Society of Chemistry peer review process and has been accepted for publication.

Accepted Manuscripts are published online shortly after acceptance, before technical editing, formatting and proof reading. Using this free service, authors can make their results available to the community, in citable form, before we publish the edited article. We will replace this Accepted Manuscript with the edited and formatted Advance Article as soon as it is available.

You can find more information about Accepted Manuscripts in the [Information for Authors](#).

Please note that technical editing may introduce minor changes to the text and/or graphics, which may alter content. The journal's standard [Terms & Conditions](#) and the [Ethical guidelines](#) still apply. In no event shall the Royal Society of Chemistry be held responsible for any errors or omissions in this Accepted Manuscript or any consequences arising from the use of any information it contains.

Cite this: DOI: 00.0000/xxxxxxxxxx

One Spiro to Shift Them All: Tuning Fluorescent Organic Nanoparticles Emission via Steric Design

Eleonore Kurek,^{a,‡} Ophélie Dal Pra,^{a,‡} Aliocha Skrzypczak,^{a,¶} Stéphane Massip,^b Jonathan Daniel,^a Mireille Blanchard-Desce,^{*a} Chloé Grazon,^{*a}

Received Date
Accepted Date

DOI: 00.0000/xxxxxxxxxx

Three quadrupolar fluorene-based dyes differing only by non-conjugated substituents form fluorescent organic nanoparticles (*d*FONs) with tunable emission from blue to yellow. A spirocyclic central substituent induces a marked red-shift via altered packing. When internalized into cells, *d*FONs evolve showing a characteristic blue-shift, enabling fluorescence-based monitoring of nanoparticle integrity and bio-imaging performance.

Bioimaging applications require probes that not only emit brightly but also report on their physical and chemical state in complex environments. Conventional fluorescent nanoparticles (NPs) - whether inorganic quantum dots or dye-doped polymer/silica NPs - are designed for stability [1, 2]. However, in the case of NPs based on supramolecular organization, such as micelles or aggregates, assessing if their structural integrity is retained within cells is trickier. Monitoring such nanoparticle disassembly usually requires multi-dye strategies or labelling approaches, which complicate synthesis and interpretation [3–6].

Fluorescent Organic Nanoparticles (FONs), and in particular dye-based FONs (*d*FONs) obtained by nanoprecipitation of dedicated π -conjugated dyes, provide a promising alternative [7, 8]. The spectral properties of *d*FONs are highly sensitive to the packing of the dye building blocks. Moreover, the fluorescence emission of *d*FONs made from polar and polarizable dyes is inherently sensitive to changes in local environment, and supramolecular organization [9]. This makes *d*FONs ideal candidates for developing self-reporting nanoprobe whose spectral response directly reflects their aggregation state.

Here, we report a family of quadrupolar dyes differing only

in their non-conjugated substituents on a fluorene core, which form self-stabilized organic nanoparticles with distinct packing geometries and emission colours. The resulting *d*FONs display strong structure-dependent spectral signatures - from blue to yellow emission - originating from different degrees of excitonic coupling features. When internalized by eukaryotic cells, the *d*FONs with strong excitonic coupling undergo a characteristic blue-shift in their emission, indicating a change in packing and environment of the constituting dyes. This demonstrates that fluorescence can serve as a direct optical readout of nanoparticle integrity, without requiring additional labelling or ratiometric design.

Three original quadrupolar dyes *dye-nC₉*, *dye-nC₄* and *dye-spiC₄* (Fig. 1a) with identical π -conjugated systems were synthesized through a three- or four step synthesis. They possess a common conjugated part, constituted by an electron-donating fluorene core, flanked by two thienyl moieties conjugated with two electron-withdrawing amide end-groups. The dyes differ only in the nature of the alkyl pending substituents in the fluorene core, with *dye-nC₉* bearing two nonyl chains, *dye-nC₄* two butyl chains and *dye-spiC₄* a spiro cycle (resulting in a spirofluorene core). The dyes are synthesized via a Pd-catalyzed Suzuki-Miyaura cross-coupling [10–12] between home-made 2,7-diiodospiro[alkyl-9,9-fluorene] (Scheme S1) and commercially available 5-carboxythiophene-2-boronic acid pinacol ester to introduce a conjugated carboxylic acid function (Scheme S2). The di-acid is then activated (Scheme S3) and reacted with benzylamine (Scheme S4 and S5) to yield the purified desired dyes with overall yields of 12%, 9% and 29% respectively for *dye-nC₉*, *dye-nC₄* and *dye-spiC₄* (¹H and ¹³C NMR spectra provided in Fig. S2-S4).

The photophysical properties of the three dyes *dye-nC₉*, *dye-nC₄* and *dye-spiC₄* were first examined in THF (Table 1, Table S2). Considering their identical conjugated systems, all three dyes share similar properties in solution; an absorption band peaking at 373 nm associated with a molar absorption coefficient ϵ^{max} at ca $68 \times 10^3 M^{-1} cm^{-1}$ and a fluorescence emission maximum of ca

^aUniv. Bordeaux, CNRS, Bordeaux INP, ISM, UMR 5255, F-33400 Talence, France; E-mail: chloe.grazon@u-bordeaux.fr, mireille.blanchard-desce@u-bordeaux.fr. ^bUniv. Bordeaux, CNRS, INSERM, IECB, UAR 3033, F-33600 Pessac, France.

† Supplementary Information available: [details of any supplementary information available should be included here]. See DOI: 00.0000/00000000.

¶ Present address: Univ Rennes, INSA Rennes, CNRS, ISCR (Institut des Sciences Chimiques de Rennes), UMR 6226, Université de Rennes, Rennes, FRANCE. ‡ These authors contributed equally to this work.



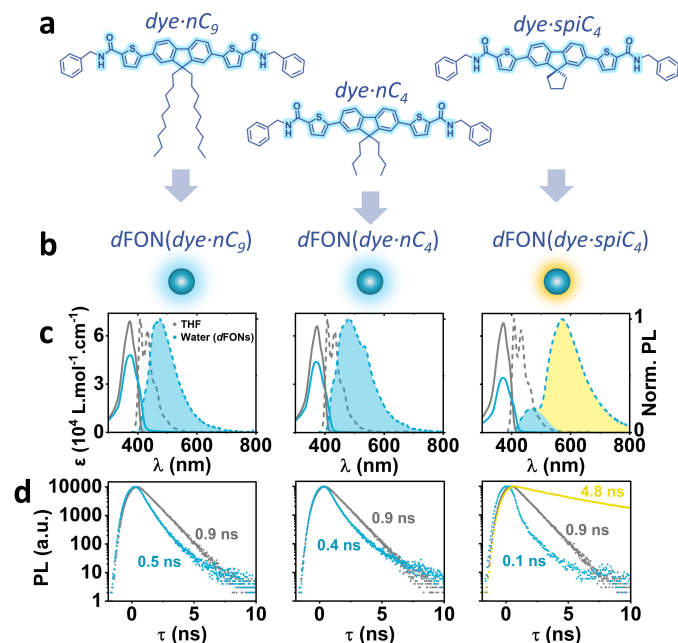


Fig. 1 a) Molecular structures of blue-emitting fluorophores *dye-nC₉*, *dye-nC₄* and *dye-spiC₄*. The grey arrows symbolize the preparation of dFONs from the dyes through nanoprecipitation in water (Fig. S1). b) Schematic representation of dFONs and their emission colour. c) Molar absorption coefficient (full lines) and normalized emission spectra upon excitation at 370 nm (dashed lines) of *dye-nC₉*, *dye-nC₄*, and *dye-spiC₄* in THF (grey) and of *dFON(dye-nC₉)*, *dFON(dye-nC₄)*, and *dFON(dye-spiC₄)* in water (blue). d) Fluorescence decays upon excitation at 370 nm of *dye-nC₉*, *dye-nC₄* and *dye-spiC₄* in THF (grey) and of *dFON(dye-nC₉)*, *dFON(dye-nC₄)* and *dFON(dye-spiC₄)* in water (blue) at 450 nm or at 590 nm (yellow), measured using time-correlated single photon counting. Fitted fluorescence lifetimes in caption.

408 nm, associated with a fluorescence quantum yield Φ_F of ca 0.70 and a fluorescence lifetime τ of 0.9 ns. The ϵ -normalized absorption spectra and normalized emission spectra of the dyes in THF are represented in grey in Fig. 1c and the solvatochromism of the dyes is depicted in Fig. S5: the three dyes exhibit no dependence of the absorption and emission spectra on solvent polarity, while the well-defined vibronic structures of the emission spectra indicates low interaction of the excited state with the solvent. This indicates that no symmetry-breaking occurs in the excited state.

The three dFONs were prepared from these three dyes using the nanoprecipitation method (Fig. S1): a 0.5 mM stock solution of dye in THF:DMSO (9:1) was added dropwise to a large volume of distilled water under magnetic stirring, such that the final proportion of organic solvent did not surpass 1%. This process yielded colourless and non-turbid colloidal dispersions of dFONs.

The photophysical properties of the resulting nanoparticles *dFON(dye-nC₉)*, *dFON(dye-nC₄)* and *dFON(dye-spiC₄)* were then investigated (Table 1, Table S2). The normalized absorption and emission spectra of the dFONs are represented in blue in Fig. 1c (full normalized spectra in Fig. S5). While the absorption spectra of *dFON(dye-nC₉)* and *dFON(dye-nC₄)* was quite similar to their molecular counterparts in THF, *dFON(dye-spiC₄)* present a 10 nm hypsochromic shift. Additionally, the molecular ϵ of

dyes as building blocks of *dFON(dye-nC₉)* and *dFON(dye-nC₄)* was ca 30% lower than that of the dyes in THF, while that for *dFON(dye-spiC₄)* was 50% lower. This hypsochromic effect, along with the slight broadening (Fig. 1c, Fig.S5) of the absorption band were reported before in closely related systems [9, 12] and were attributed to excitonic splitting [15, 16]. The most striking differences by far are found in the dFONs emissive properties. Compared to the molecular dyes in solution, all dFONs display a broadened and bathochromically shifted emission, with a loss of vibronic structure (Fig. 1c, Table 1). *dFON(dye-nC₉)* and *dFON(dye-nC₄)* emission spectra are not identical but close, with an emission at 475 nm and 481 nm respectively. The spectral shape of *dFON(dye-nC₄)* is slightly broader and displays a small additional shoulder around 540 nm. These observed changes in the shape, position, and intensity of the emission spectrum are a common occurrence in dFONs, due to intermolecular interactions. In addition, the fluorescence quantum yields (Φ_F) of *dFON(dye-nC₉)* ($\Phi_F = 0.23$) and *dFON(dye-nC₄)* ($\Phi_F = 0.15$) are lower than that of the dyes in THF solutions. This trend arises from two key factors: a slight reduction in the radiative rate constant (k_r) in relation with interchromophoric interactions within the aggregated dFONs, and a marked increase in the non-radiative rate constant (k_{nr}) (Table 1, Fig. S6), which might be ascribed to vibrational deactivation due to water molecules in close proximity to the surface of the nanoparticle [17]. We also stress that the fluorescence emission of crystals of *dye-nC₉* and *dye-nC₄* does not overlap with the corresponding dFONs spectra (Fig. S8), suggesting the amorphous nature of these molecular aggregates.

In comparison, *dFON(dye-spiC₄)* emissive properties are strikingly different: the spectrum comprises a main band at 569 nm, and a minor band (about 15% of the main band in height) at 466 nm, resembling that of *dFON(dye-nC₉)* and *dFON(dye-nC₄)*. Concomitantly, the fluorescence quantum yield is drastically reduced, down to 0.03, and the fluorescence lifetime is significantly increased to 4.8 ns at 590 nm (Fig. 1d, Fig. S6-S7). We attribute this new band in the yellow region to strong excitonic coupling [16, 18], which stabilizes a low-energy emissive state, thus reducing k_r and enhancing k_{nr} and resulting in reduced brightness. The fact that only *dFON(dye-spiC₄)* exhibit this band indicates that the rigid nature of the spiro substituent and its small size play a crucial role, by strongly affecting molecular packing within dFONs. This showcases the importance of the nature of the substituents in dye design for dFONs [9, 19].

For comparison, a dye bearing the same spiro substituent but with benzyl-amide groups replaced by diethyl-imide groups (*dye-spiC₄NEt₂* (6), Scheme S6, Fig. S5-7, Tables S1-2) [12] exhibits only a weak red shoulder in its emission. In addition, the crystal structures of *dye-spiC₄* and *dye-spiC₉* (Fig. S11-S12 and Tables S3-S4) indicate that the benzyl-amide groups could play a role in the molecular arrangement of the dyes. This suggests that, beyond the spiro unit promoting closer dye proximity compared to extended alkyl chains, the benzyl-amide groups at the dye termini may also modulate the spatial organization of the dyes within dFONs, thereby influencing their optical properties. The effective Stokes Shift of *dFON(dye-spiC₄)* is huge compared to that of *dFON(dye-nC₉)* and *dFON(dye-nC₄)* ($10 \times 10^3 \text{ cm}^{-1}$ com-



Table 1 Photophysical and structural properties of the three dyes in THF and of the associated *dFONs* in water, at 20°C.

Sample	Solvent	$\lambda_{\text{abs}}^{\text{max, a)}$ nm	$\epsilon^{\text{max, b)}$ $\times 10^3 \text{ M}^{-1} \text{ cm}^{-1}$	$\Delta_{\text{v}}^{\text{c)}$ cm^{-1}	$\lambda_{\text{em}}^{\text{max, d)}$ nm	$\Phi_{\text{F}}^{\text{e)}$	$\tau_{\text{amp}}^{\text{f)}$ ns	$k_{\text{r}}^{\text{g)}$ ns^{-1}	$k_{\text{nr}}^{\text{h)}$ ns^{-1}	$B_{\text{V}}^{\text{i)}$ $\times 10^3 \text{ M}^{-1} \text{ cm}^{-1} \text{ nm}^{-3}$
<i>dye-nC9</i>	THF	373	69 ± 8	2300	408	0.72 ± 0.02	0.9	0.8	0.3	35
<i>dFON(dye-nC9)</i>	H ₂ O	374	48 ± 8	5685	475	0.23 ± 0.01	0.5	0.5	1.5	8
<i>dye-nC4</i>	THF	373	66 ± 2	2360	409	0.65 ± 0.03	0.9	0.7	0.4	36
<i>dFON(dye-nC4)</i>	H ₂ O	370	44 ± 2	6237	481	0.15 ± 0.01	0.4	0.4	2.1	6
<i>dye-spiC4</i>	THF	372	68 ± 2	2372	408	0.70 ± 0.03	0.9	0.8	0.3	44
<i>dFON(dye-spiC4)</i>	H ₂ O	362	34 ± 2	10050	569 (466)	0.03 ± 0.01	0.1/4.8*	0.1/0.01*	10/0.2*	0.9

A more comprehensive version of this table is provided in the Supporting Information (Table S1). (a) Absorption maximum wavelength; (b) Molar absorption coefficient of the dyes at $\lambda_{\text{abs}}^{\text{max}}$ (in solution in THF or as *dFONs* subunits), measured from three differently prepared solutions and subsequent dilutions (error bars correspond to the standard deviation on all points); (c) Stokes shift; (d) Emission maximum wavelength; (e) Relative fluorescence quantum yield, using references: Quinine bisulfate in H₂SO₄ 0.5 M ($\Phi_{\text{F}} = 0.546$) [13] and 4-(dicyanomethylene)-2-methyl-6-[p-(dimethyl-amino) styryl]-4H-pyran in EtOH ($\Phi_{\text{F}} = 0.437$) [14]. Error bars correspond to the standard error on the linear regression; (f) Amplitude-averaged fluorescence lifetime, using $\lambda_{\text{exc}} = 370$ nm and $\lambda_{\text{em}} = 450$ nm, except for (*): $\lambda_{\text{em}} = 590$ nm; (g) Radiative rate constant; (h) Non-radiative rate constant; (i) Brightness per volume. All steady-state fluorescence emission spectrum were recorded using $\lambda_{\text{exc}} = 370$ nm.

pared to $6 \times 10^3 \text{ cm}^{-1}$).

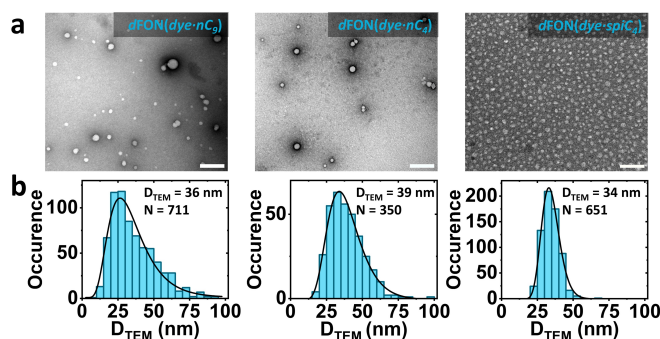


Fig. 2 a) Transmission electron microscopy images of *dFON(dye-nC9)*, *dFON(dye-nC4)* and *dFON(dye-spiC4)*, negatively stained using uranyl acetate. Scale bar: 200 nm; b) Size distribution of *dFONs* dry diameters measured from TEM images. Captions: resulting mean dry diameters of *dFONs* (D_{TEM}) and number of measured particles (N). Note that for *dFONs(dye-spiC4)*, only spherical nanoparticles were counted for the size distribution.

The morphological characteristics of *dFONs* were investigated using transmission electron microscopy (TEM), as illustrated in Fig. 2 and Fig. S9. *dFON(dye-nC9)* and *dFON(dye-nC4)* appeared as spherical nanoparticles with mean diameters of 35-40 nm. *dFON(dye-spiC4)* were found to exhibit polymorphism, with one population of spherical nanoparticles, averaging *ca* 35 nm in diameter and a second population of "rod-like" particles, measuring roughly 20 nm in width and from 20 up to 150 nm in length.

The average number of dyes per nanoparticles (N , Eq. S1) is derived from the *dFONs* dry diameter. The theoretical brightness (B , Eq. S4, Table S1, Fig. S10) and brightness per volume (B_{V} , Eq. S5, Table 1) of the NPs are then calculated. While *dFON(dye-nC9)* and *dFON(dye-nC4)* have a similar brightness around $2 \times 10^8 \text{ M}^{-1} \text{ cm}^{-1}$, the brightness of *dFON(dye-spiC4)* is ten times lower ($2 \times 10^7 \text{ M}^{-1} \text{ cm}^{-1}$). This resulted in brightnesses per volume around $7 \times 10^3 \text{ M}^{-1} \text{ cm}^{-1} \text{ nm}^{-3}$ for *dFON(dye-nC9)* and *dFON(dye-nC4)* and $0.9 \times 10^3 \text{ M}^{-1} \text{ cm}^{-1} \text{ nm}^{-3}$ for *dFON(dye-spiC4)*. The B_{V} of *dFONs* containing dyes with alkyl chains is approximately ten times higher than that of PMMA nanoparticles doped with blue-emitting cyanine ($B_{\text{V}} = 7 \times 10^2 \text{ M}^{-1} \text{ cm}^{-1} \text{ nm}^{-3}$) for NPs of com-

parable size [20]. In contrast, *dFON(dye-spiC4)* exhibit a 100-fold higher overall brightness compared to QD540 ($B = 1.7 \times 10^5 \text{ M}^{-1} \text{ cm}^{-1}$) [21], while showing a similar brightness per unit volume ($B_{\text{V, QD540}} = 1.5 \times 10^3 \text{ M}^{-1} \text{ cm}^{-1} \text{ nm}^{-3}$), which can be attributed to the smaller size of bare QDs.

Finally, before using these nanoparticles in biological applications, their colloidal stabilities in different media (water or cell culture medium) were evaluated (Fig. S13). Over 24 hours, neither a change in absorbance nor setting was observed. This confirms the good colloidal stability of the *dFONs* in such conditions and supports their potential use in cell culture medium. In addition, the emissive properties of the *dFON(dye-spiC4)* were evaluated in supplemented cell culture media (DMEM+FBS) (Fig. S14). Overall the emissive spectra remain the same, but a decrease of the band at 570 nm and an increase of the band at 466 nm is observed.

dFON(dye-spiC4) were then evaluated as bioimaging probes in fluorescence microscopy experiments on HEK and COS-7 cells (Fig. 3, Fig. S15 and S16). First, the *dFONs* were incubated with HEK cells in DMEM supplemented with 10% FBS. Live, wash-free imaging was then conducted over one hour to monitor the intracellular fate of the nanoparticles. Under these conditions, only the *dFONs* that had entered or were concentrated inside the cells could be detected, whereas dispersed nanoparticles in the culture medium remained below the detection threshold.

After approximately one hour, the *dFONs* accumulated inside the cells and displayed an emission band with a maximum around 460 nm (Fig. 3). This emission does not overlap with that of the *dFONs* in DMEM+FBS, nor with that of the isolated *dye-spiC4* in a polar solvent such as DMSO. Instead, it closely resembles the emission of *dFON(dye-nC4)* or *dFON(dye-nC9)*. To further investigate this unexpected behaviour, the intracellular accumulation of *dFON(dye-spiC4)* was monitored at *ca* 30, 40, 50 and 90 min (Fig. S15). Remarkably, the nanoparticles entered the cells rapidly, within *ca* 30 min, and continued to accumulate over the full duration of the experiment. Concomitantly, the fluorescence emission of *dFON(dye-spiC4)* underwent a pronounced hypsochromic shift.

We hypothesize that upon cell internalization, the *dFONs* undergo a structural reorganization within the cellular environment while remaining in an aggregate state. Such a reorganization



would account for the loss of excitonic coupling signatures, while maintaining an emission profile characteristic of aggregated dyes rather than isolated chromophores.

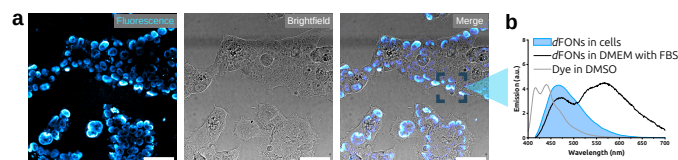


Fig. 3 a) Fluorescence microscopy images of *dFON(dye-spiC₄)* at 5 nM in live HEK cells in DMEM+10%FBS cell-culture medium (incubation time= 54 min.). Scale bar: 50 μm . λ_{exc} =405 nm, λ_{em} = 415 nm - 500 nm. b) Raw *in cellulo* emission spectra of *dFON(dye-spiC₄)* within the cells (blue), overlaid on the corresponding normalized emission spectra of *dFONs* in DMEM with FBS (10%, black) and of the dye in solution in dimethylsulfoxide (DMSO, grey).

To assess whether this behavior was cell-line dependent, we also incubated *dFON(dye-spiC₄)* with COS-7 cells and imaged them after 2h (Fig. S16). Strikingly, the fluorescence signal was again centered around 450 nm and the excitonic coupling signature was lost. These observations indicate that the *dFONs* exhibit the same intracellular behavior regardless of the cell line investigated (fibroblast or embryonic).

Our study demonstrates that a single substituent modification on a dye can drastically alter its solid-state properties, leading in our case to a pronounced red-shift in emission. This unique spectral signature provides an efficient means to monitor the aggregation state of fluorophores within nanoparticles without the need for mixed-dye systems - an important asset for applications such as biosensing or drug-delivery, where controlling nanoparticle behaviour is essential. In living cells, *dFON(dye-spiC₄)* display a markedly broadened and blue-shifted emission compared to *dFONs* in aqueous suspension, a behaviour that indicates a loss of excitonic coupling promoted either by the dissociation of the nanoaggregates (as previously observed for other *dFONs* [3]) or by reorganization of the dyes within the assemblies. What makes this system truly innovative is its reliance on a single dye component, which—despite its simplicity—achieves dramatic fluorescence signal modulation in cells. This modulation is driven entirely by the dynamic reorganization of the dyes within the nanoparticle, rather than the conventional "off/on" mechanisms seen in most systems (where fluorescence is quenched in aggregated states and only recovers upon nanoparticle dissolution in biological media) [22] or solvatochromic effects, where the dissolution of the nanoparticles is followed by a change in the fluorescence signal [23]. Importantly, the optical tuning is achieved here while preserving the nanoparticle features associated with high brightness. Such sensitivity to the cellular environment, combined with distinct staining profiles across cell lines, highlights that the nature of the dye substituents has a strong influence on the cellular fate of *dFONs* (as already demonstrated for other systems [9, 24]) and further supports their potential for controlled sensing [12] and drug-delivery applications [25].

Author Contributions

CRediT: Eleonore Kurek: investigation, validation, methodology, visualisation, writing - original draft preparation. Ophélie Dal Pra: investigation, visualisation, writing - review & editing. Aliocha Skrzypczak: investigation, Writing - Review & Editing. Stéphane Massip: investigation, data curation. Jonathan Daniel: investigation, visualization, writing - review & editing. Mireille Blanchard-Desce: conceptualization, funding acquisition, supervision, writing - review & editing. Chloé Grazon: conceptualization, data curation, funding acquisition, methodology, project administration, supervision, visualisation, writing - original draft preparation.

Conflicts of interest

There are no conflicts to declare.

Data availability

Data for this article are available at Zenodo repository 18324973, except for crystals data accessible on CCDC repositories 2524470 and 2524471.

Acknowledgments

The synthesis of dyes 5b and 6 were performed by J. Traisnel and A. Okba respectively. This project has received funding from the European Research Council (ERC) under European Union's Horizon Europe research and innovation program (Grant agreement N° 101077364). Financial support for ODP and EK was provided through the MENESR (Ministère de l'Education Nationale, de l'Enseignement Supérieur et de la Recherche) of France. This work has also benefited from the the LIGHT S&T Graduate Program (PIA 3 Investment for Future Program, ANR-17-EURE-0027), support and facilities and expertise of IECB Biophysical and Structural Chemistry platform (BPCS), CNRS UAR3033, Inserm US001, Univ Bordeaux. Continuous support from the university of Bordeaux, Bordeaux-INP and CNRS is greatly acknowledged.

References

- (1) W. R. Algar, A. Szwarczewski and M. Massey, *Analytical Chemistry*, 2023, **95**, 551–559.
- (2) W. R. Algar, M. Massey, K. Rees, R. Higgins, K. D. Krause, G. H. Darwish, W. J. Peveler, Z. Xiao, H.-Y. Tsai, R. Gupta, K. Lix, M. V. Tran and H. Kim, *Chemical Reviews*, 2021, **121**, 9243–9358.
- (3) J. Boucard, T. Briolay, T. Blondy, M. Boujtita, S. Nedellec, P. Hulin, M. Grégoire, C. Blanquart and E. Ishow, *ACS Applied Materials & Interfaces*, 2019, **11**, 32808–32814.
- (4) N. Curtin, M. Garre, J.-B. Bodin, N. Solem, R. Méallet-Renault and D. F. O'Shea, *RSC Advances*, 2022, **12**, 35655–35665.
- (5) M. Zhang, C. Wang, C. Yang, H. Wu, H. Xu and G. Liang, *Analytical Chemistry*, 2021, **93**, 5665–5669.
- (6) S. W. Morton, X. Zhao, M. A. Qadir and P. T. Hammond, *Biomaterials*, 2014, **35**, 3489–3496.



- (7) V. Parthasarathy, S. Fery-Forgues, E. Campioli, G. Recher, F. Terenziani and M. Blanchard-Desce, *Small*, 2011, **7**, 3219–3229.
- (8) S. Fery-Forgues, *Nanoscale*, 2013, **5**, 8428–8442.
- (9) J. Daniel, O. D. Pra, E. Kurek, C. Grazon and M. Blanchard-Desce, *Comptes Rendus. Chimie*, 2024, **27**, 1–17.
- (10) J. Daniel, A. G. Godin, M. Palayret, B. Lounis, L. Cognet and M. Blanchard-Desce, *Journal of Physics D: Applied Physics*, 2016, **49**, 084002.
- (11) H. Li, J. Daniel, J.-B. Verlhac, M. Blanchard-Desce and N. Sojic, *Chemistry – A European Journal*, 2016, **22**, 12702–12714.
- (12) O. Dal Pra, J. Daniel, G. Recher, M. Blanchard-Desce and C. Grazon, *Small Methods*, 2024, **8**, 2400716.
- (13) D. F. Eaton, *Pure and Applied Chemistry*, 1988, **60**, 1107–1114.
- (14) K. Rurack and M. Spieles, *Analytical Chemistry*, 2011, **83**, 1232–1242.
- (15) M. Kasha, H. R. Rawls and M. Ashraf El-Bayoumi, *Pure and Applied Chemistry*, 1965, **11**, 371–392.
- (16) A. S. Davydov, *Soviet Physics Uspekhi*, 1964, **7**, 145.
- (17) J. Maillard, K. Klehs, C. Rumble, E. Vauthey, M. Heilemann and A. Fürstenberg, *Chemical Science*, 2021, **12**, 1352–1362.
- (18) J. Gierschner, J. Shi, B. Milián-Medina, D. Roca-Sanjuán, S. Varghese and S. Park, *Advanced Optical Materials*, 2021, **9**, 2002251.
- (19) J. Daniel, These de doctorat, Bordeaux, 2015.
- (20) P. Ashokkumar, N. Adarsh and A. S. Klymchenko, *Small*, 2020, **16**, 2002494.
- (21) R. Gupta, W. J. Peveler, K. Lix and W. R. Algar, *Analytical Chemistry*, 2019, **91**, 10955–10960.
- (22) J. Boucard, C. Linot, T. Blondy, S. Nedellec, P. Hulin, C. Blanquart, L. Lartigue and E. Ishow, *Small*, 2018, **14**, 1802307.
- (23) A. Faucon, H. Benhelli-Mokrani, L. A. Córdova, B. Brulin, D. Heymann, P. Hulin, S. Nedellec and E. Ishow, *Advanced Healthcare Materials*, 2015, **4**, 2727–2734.
- (24) A. H. A. M. v. Onzen, L. Albertazzi, A. P. H. J. Schenning, L.-G. Milroy and L. Brunsveld, *Chemical Communications*, 2017, **53**, 1626–1629.
- (25) A. Jana, K. S. P. Devi, T. K. Maiti and N. D. P. Singh, *Journal of the American Chemical Society*, 2012, **134**, 7656–7659.



Data availability statement

View Article Online
DOI: 10.1039/D5CC06995E

Data for this article are available at Zenodo repository 18324973, except for crystals data accessible on CCDC repositories 2524470 and 2524471

